A Novel 3D-Overlap Metric for Medical Volume Images

Badera Abu-Rumman
Al-Balqa Applied University
Salt, Jordan

Zainab Al-Rahamneh
Al-Balqa Applied University
Salt, Jordan

Asma'a Khtoom
Al-Balqa Applied University
Salt, Jordan

Mohammad Ryalat
Al-Balqa Applied University
Salt, Jordan

ABSTRACT
It is customary to measure the correctness of 3D medical segmentation of images and registration. As a result, the effectiveness and dependability of the used overlap metric are crucial to the evaluation process. A novel 3D-overlap metric for medical volume imaging is presented in this research. The proposed metric is specifically created to be orientated for medical volume images, unlike the present overlap metrics used in biomedical domains, which were primarily built for computer graphics applications. The peoposed complementary overlap metric furnishes statistically robust data, enabling visualization and analysis of the scale and localization of matching and mismatching volumes in addition to the merit number of the fraction of the region match. This metric is practical for medical images since it provides particular values for the axial, sagittal, and coronal planes. To guarantee reliability and generalizability in this work, six distinct datasets were employed for comprehensive assessment. To assess the proposed metric, two methods were employed. The first step is to look at the association between the proposed overlap metric and other, more commonly used and recognized overlap metrics. The second involves examining the results of the proposed metric for specific test instances where we are aware of the expected trend of the right outputs in advance. The findings demonstrate the value of applying the proposed overlap metric to assess how well medical image segmentation and registration performed.

General Terms
Image Segmentation, Medical Images, Biomedical Engineering.

Keywords
Overlap Metric, Segmentation, 3-D Medical Images, Axial, Sagittal, Coronal, Volume of Match.

1. INTRODUCTION
Medical images are commonly constructed from a pile of 2D slices attained by Computed Tomography (CT), Magnetic Resonance Imaging (MRI), or Micro-CT scans. The proportion of overlap between two data sets is determined using the Three Dimensional (3D) overlap metric.

The degree, to which the results of a registration between images or image segmentation match with the actual data, or a so-called "gold standard", is referred to as accuracy [1]. Reliable and precise overlap metrics are indispensable tools for driving success in biomedical engineering. The quality of the registration and segmentation operations will be reflected by this metric, which should quantify the region agreement between two volume images.

In medical applications, the precision of the image registration and segmentation operations is crucial. A variety of techniques are used in registration to establish anatomical or functional correlation between images taken at various periods, using various modalities, or of various subjects [2] [3]. For image-guided radiosurgery, images registration is crucial [4]. Image registration facilitates interventional procedures through accurate alignment of pre-interventional (e.g., planning CT) and intra-procedural (e.g., real-time fluoroscopy) data across diverse applications like interventional radiology, radiation therapy, and minimally invasive surgery [5-9]. Additionally, in anabolic and catabolic mouse models, 3D image registration increases the long-term precision of in vivo Micro Computed Tomographic measures [10].

One of the most fundamental processes needed in medical applications is image segmentation. The ability of image segmentation to define, describe, and visualize regions of interest in medical images is what gives it its significance [11]. Image segmentation is generally required to fully utilize the medical imaging generated by contemporary imaging modalities like CT and MRI. Medical image segmentation methodologies encompass manual, automated, and hybrid approaches. Despite the substantial accuracy gains enabled by computer-aided techniques, manual segmentation remains susceptible to inter-observer variability and incurs significant time expenditure [12] [13]. A trustworthy overlap metric is required for both human and machine segmentation methods in order to evaluate the effectiveness of the segmentation procedure. If the right measures for measuring region agreement are available, registration and segmentation can be evaluated numerically [14].

Academics extensively employ (1) MSDE which stands for Mean Surface Distance Error, (2) HD stands for Hausdorff Distance, and (3) SDCCV stands for Signed Distances with Colour-Coded Visualization to quantify surface overlap in medical volume images. Both MSDE and SDCCV leverage Euclidean distance for point-wise comparisons, albeit with SDCCV generating signed values and color visualizations. Notably, MSDE and SDCCV exhibit significant conceptual overlap, as evidenced by their interchangeable usage in numerous studies [15–22].

2. CONTRIBUTION
The intensive review and investigation that were performed by the authors of this research regarding the current overlap measurements lead us to several findings:

– The result is not quantified as a single number by signed distances with color-coded visualization (i.e. figure of merit).

– These overlap measurement techniques, initially conceived for general applications and specifically for computer graphics, have demonstrated significant efficacy in the context of medical image registration.

– While metrics like HD, MSDE, and SDCCV provide surface-level insights, more comprehensive assessments necessitate voxel-based approaches for a deeper understanding of internal overlap.

– MSDE and SDCCV are characterized as distance-based measures more so than overlap-based metrics because they are sensitive to point placements [29].

– Medical images frequently contain outliers [30] which HD is sensitive to.

– HD occasionally delivers erroneous results because it finds the "furthest near neighbor" between two sets – the largest distance separating the closest points in each set.

– Traditional distance-based error metrics can mask significant discrepancies on highly curved surfaces, even if the actual geometric discrepancy is significant. This is because they only consider the closest points between surfaces, potentially overlooking deeper misalignments [31].

– Those measurements based on distance instead yield an absolute figure that indicates the average distances rather than a percentage of overlap.

– None of those overlap measures provide an analysis of the axial, sagittal, and coronal planes, despite the fact that this analysis is crucial in several clinical situations.

A novel 3D-overlap metric is presented in this paper. This metric goes beyond the final score. It provides additional statistical data that helps visualize the size and location of matching and mismatching regions. This is like having a detailed map of the overlap, not just a single percentage. This additional information is crucial for surgeons, researchers, and anyone who needs to understand the nuanced differences between medical images.

The proposed metric is not just a single number. It is a framework that can measure overlap in three key scenarios:

Surface-to-surface: Comparing the outer shell of two organs, like brain hemispheres.

Surface-to-volume: Matching a segmented tumor against the entire scanned area.

Volume-to-volume: Comparing entire organ shapes, like lungs or hearts.

The overlap ratio is examined using the axial, sagittal, and coronal planes by the provided overlap measure. As a result, it is a good option for volume imaging in medicine. It is crucial to not only calculate global measures but also examine how these mistakes are distributed locally, as local distributions may quickly reveal which anatomical shapes are mismatched and where [25]. The overlap metric's complimentary values provide the ability to identify which sections are mismatched or incorrectly matched and where they are.

Additionally to what was previously said, the presented overlap metric is insensitive to outliers because the Dice metric is employed internally as it will be shown in Section 3. The proposed overlap-focused metric excels at identifying irregularities on exceedingly curved surfaces, especially if "image fill" option is disabled. This powerful capability, further explained in Section 3, comes with a trade-off.

3. MATERIALS AND METHODS

3.1 Datasets

This study explores six diverse datasets (Figure 1). The first, from pelvic CT scans [32], presents a surface in Figure 1(a) saved as an STL file. Similarly, Figure 1(b) showcases a knee surface from CT data [33], also saved in STL format.

Datasets 3 and 4 in Figure 1 depict three-dimensional printed objects: a set of nested cubes, displayed in Figure 1(c), and a dome, displayed in Figure 1(d). The two objects were digitally fabricated with specific sizes and subsequently a 3D printer is employed at the University of East Anglia's Computing Sciences School's 3D printing laboratory to print these objects. CT data files for those two objects were obtained at Ipswich Hospital in the United Kingdom. Both objects were scanned with a handheld laser scanner as well. Figure 2(a) and (b) exhibit photographs of the real plastic objects utilized in this investigation, while Figure 2 objects(c) and (d) show a CT slice for each object. Figure 2(e) objects depicts the hand-held laser scanner that was employed to photograph the two objects.

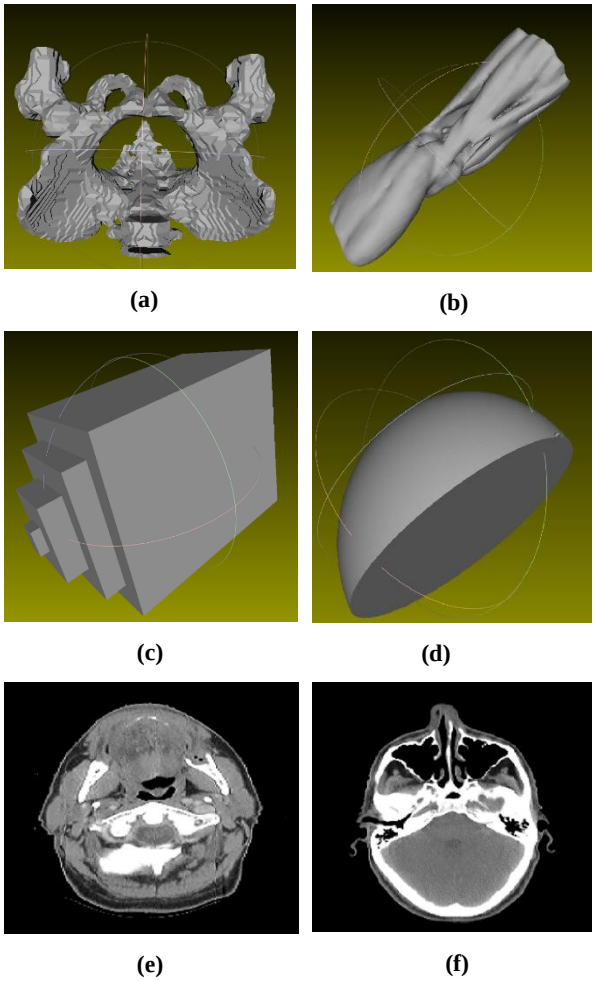

Fig 1: This study made use of six separate data sets.

The final two datasets (Figure 1(e) and (f)) were retrieved from the Cancer Imaging Archive [34,35]. They comprise groups of CT images acquired from head scans of two individuals.

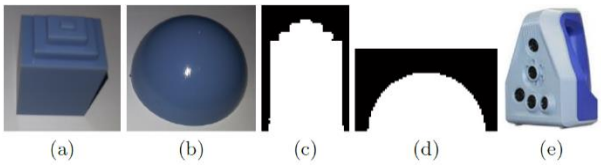

Fig 2: The experiment utilized plastic objects in cubic and dome geometries (a) and (b). All of objects were photographed with an AS Spider TM laser scanner (e). CT image slices are presented in (c) and (d).

3.2 Methods

The provided overlap metric, depicted in Figure 3, quantifies how much two 3D models overlap. Two medical volume images are accepted as inputs. In light of this, the method chooses one of three paths to calculate the overlap percentage. The first one illustrates the situation where both inputs are surfaces. In medical imaging, comparing surfaces acquired from the same object using different devices or validating 3D model segmentation against a ground truth surface are frequent use cases, as documented in [36–39]. The next path characterizes the scenario where the first input is a surface and the second input is a discrete volumetric representation (i.e., 3D grid). A situation where this is necessary is when a CT derived model needs to be evaluated by being compared to a ground truth (i.e. surface mesh) [9,40–44]. The third path reflects the scenario in which both inputs are a 3D voxel grid. Comparing CT scans generated by different scanners for the same object exemplifies this scenario of assessing surface overlaps across modalities. [45–46].

The proposed model will first extract the isosurface to create a surface. A widely used method known as the marching cubes algorithm performs this extraction [47]. Following that, each surface in each of the three planes is intersected by a plane/triangle to begin the slicing process (i.e. axial, sagittal and coronal). The three following steps make up the majority of the slicing process:

– Mesh simplification
– Intersecting planes and triangles
– Intersection points are projected onto 2D image pixels.

4. EXPERIMENTAL WORKS

This research delves deep into the reliability of the proposed innovative 3D overlap metric. A series of experiments were conducted to rigorously assess its accuracy in diverse scenarios. These experiments will answer crucial questions:

- Can the proposed metric accurately quantify overlap across different types of 3D data (surfaces and volumes)?
- How reliable are the conclusions drawn from the metric in various comparison scenarios?
- What are the limitations of the metric, and how can they be addressed?

By delving into these questions, the aim to refine and validate the proposed 3D overlap metric, ensuring it becomes a valuable tool for diverse medical applications. Table 1 shows the results of applying the proposed overlap metric for different cases and Table 2 shows the results of applying RMSE, and HD for the same different cases.

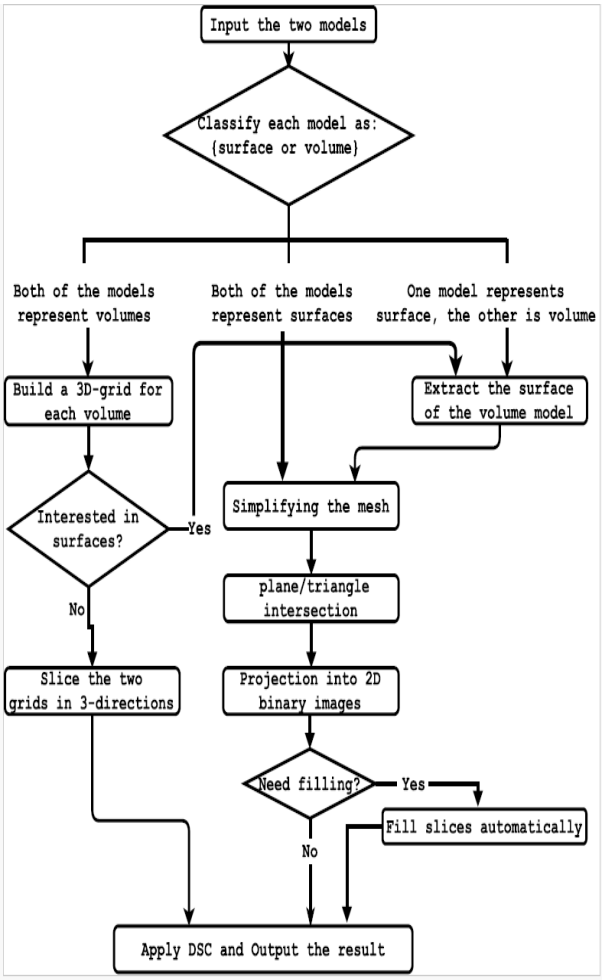

Fig 3: The proposed model.

Table 1. Quantifying overlap across axial, sagittal, and coronal views in various test cases.

T.Case	Axial	Sagittal	Coronal	Avg.
1	1.0000	1.000	1.000	1.000
2	0.91849	0.87023	0.8983	0.8957
3	0.86423	0.87877	0.8608	0.8679
4	0.86566	0.83477	0.88539	0.8619
5	0.82493	0.79827	0.82531	0.8162
6	0.8131	0.77446	0.7899	0.7925
7	0.71122	0.75858	0.70818	0.726
8	0.72988	0.68254	0.76811	0.7268
9	0.65774	0.64804	0.64529	0.6504
10	0.54668	0.50139	0.51741	0.5218
11	0.43425	0.50979	0.40788	0.4506
12	0.42622	0.38793	0.46384	0.426
13	0.34392	0.33966	0.319	0.3342
14	0.87093	0.79052	0.87813	0.8465
15	0.77063	0.6625	0.78236	0.7385
16	0.11866	0.087385	0.13057	0.1122
17	0.000	0.000	0.000	0.000

Table 2. RMSE and HD measurements for different test cases.

Case#	RMSE	HD
1	0.000	0.000
2	0.7981	1811
3	0.9859	2531
4	0.9144	2597
5	1.2269	2490
6	1.4078	1871
7	1.6659	2549
8	1.6831	2544
9	2.1291	2501
10	3.0101	1985
11	4.1092	2635
12	4.1253	2533
13	5.3131	2564
14	0.9858	99
15	1.7848	248
16	7.6134	1240
17	64.3856	8846

5. DISCUSSION

A screenshot of the Matlab GUI tool which was developed to execute and evaluate the proposed 3D-overlap metric is shown in Figure 4. Some of the observations we're going to talk about here were reported in Tables 1 and 2. The first finding is that the values produced by the proposed overlap metric are connected with the findings of the RMSE measure, which is one of the most extensively used metrics in a huge number of studies. The proposed metric's dependability is further supported by this correlation. The second finding is that the proposed metric's results, as shown in those two tables, make sense in terms of geometry and transformation. A positive correlation exists between the rotation angle of an object and the decrease in its similarity ratio. This can be observed, for example, in a comparison of object rotations of 2 degrees, 5 degrees, and 15 degrees, where the similarity ratio consistently decreases with increasing angle. (rows#5, #9, and #13 in Table 1 are examples).

Another illustration of the rationality of the results is that when an object is translated by 2 percentage points, it is more similar than when it is translated by 5 percentage points, and the latter is more similar than when it is translated by 25 percentage points (see as an example rows #14 to #16 in Table 1). The final finding is that any other alignment procedure may be helped to achieve better alignment by using the complimentary values produced by the proposed metric to identify the source of the discrepancy. Translating the object in the y-direction notably decreases the similarity ratio in that view compared to axial and coronal views (Table 1, rows #14–#16). Conversely, rotating around the x-axis significantly increases the similarity ratio in the axial view relative to sagittal and coronal perspectives.

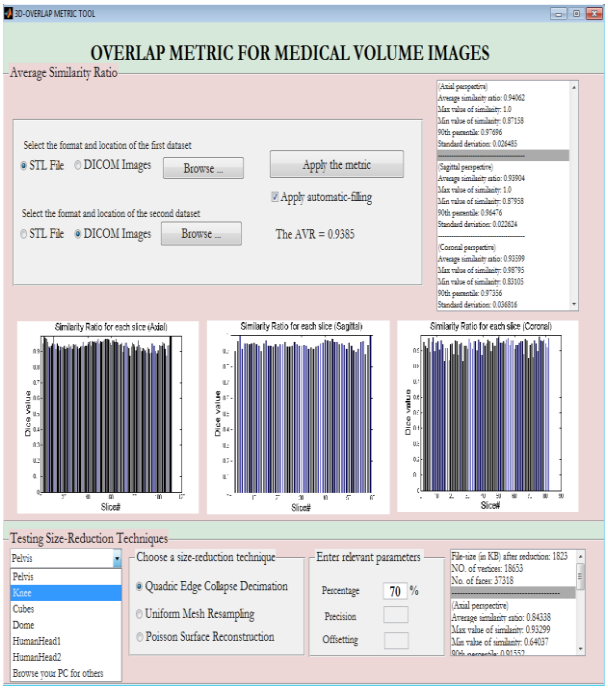

Fig 4: A screenshot of the GUI tool that prepared using Matlab

As shown in Figure 5, the proposed overlap metric can handle the partial volume impact scenario. This is due to the fact that the proposed overlap metric accounts for three views when calculating the degree of overlap. This produces partial volume estimates that are more precise. The proposed metric offers the standard deviation as an additional reading. When the standard deviation (SD) is high, the degree of similarity between the respective images is likely to be dispersed across a large range of values. This implies that there are some outliers, and it is important to identify the images that are to cause by looking at the figures that show the degree of similarity slice by slice.

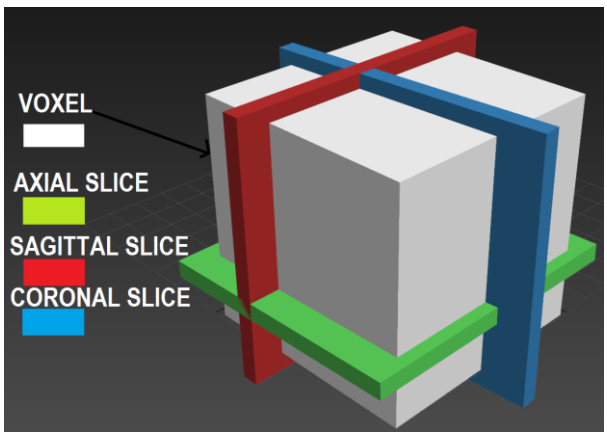

Fig 5: Three view triangulation in voxel space yields accurate partial volume estimates.

The proposed metric's axial, sagittal, and coronal analysis data can be used to identify locations or positions with lower overlap or mismatch. For instance, the proposed metric generates the bar charts displayed in Figure 6 to determine the percentage of overlap for a head. Figure 7(a) illustrates a delineation of that head in order to make things clearer (a). A segmentation of the volume into 102 axial, 61 sagittal, and 74 coronal slices was performed. Figure 5 charts visualize similarity across these slices. The left half of the head (red in Figure 7b) exhibits low

similarity. This misalignment was observed in the sagittal view's first half (30 images) and the axial view's first 20% (20 images). Notably, the coronal view displays consistent similarity, suggesting the issue isn't specific to a particular region along the front-to-back axis.

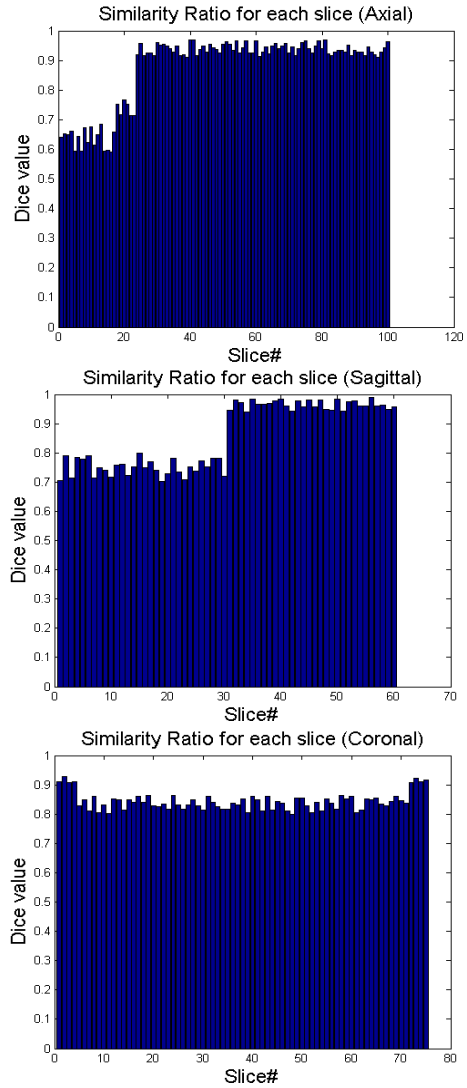

Fig 6: Bar charts generated by the proposed metric for a head: axial, sagittal, and coronal views sorted from top to left

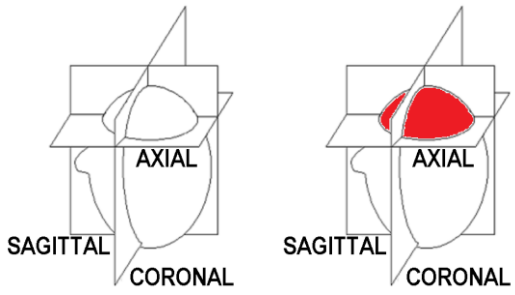

(a) (b)

Fig 7: (a) Delineating the head's boundaries across three key planes: axial (horizontal), sagittal (side), and coronal (frontal). (b) A specific region with low overlap is highlighted in red.

6. CONCUSION

Degree of similarity between medical volume images was measured in three dimensions using a new model that was given in this paper. The characteristic of image segmentation and registration is quantified in part by the use of the presented metric. It has several properties, the first of which is that by going beyond a single number, metric empowers medical professionals with deeper insights into their 3D medical data. Second, it takes one surface and one three-dimensional grid or two surfaces and two three-dimensional grids as inputs. Moreover, it provides supplementary statistical data that may be used to identify the quantity and locations of zones of match and mismatch. It is practical for medical applications since, among other things, it analyses the degree of similarity while considering the 3-D planes. Fifth, it is insensitive to outliers, making this statistic especially crucial for medical pictures. Sixthly, it is not necessary to orient or place the undervalued goods in a particular attitude. In addition to what has already been discussed, it is also capable of finding geometric faults on extremely curved surfaces. It just accepts the two items as they are and begins the evaluation without the need for any initialization or special settings.

The results of the presented metric have been rigorously examined using six different data sets and a variety of test cases. A comparison is performed between the values produced by the proposed 3D overlap metric to the values produced by three other frequently used overlap metrics. The results of the proposed overlap metric are clearly correlated and logical. The proposed overlap measure is useful for medical volume images because, according to the thorough analysis that was presented in this research, it provides complimentary output that define the regions of overlaps with respect to the 3-D perspectives.

Down-sampling medical images necessitates a balance between resource efficiency and detail preservation. This study leverages a novel overlap metric to optimize down-sampling for Poisson Surface Reconstruction (PSR), Uniform Mesh Resampling (UMR), and Quadric Edge Collapse Decimation (QECD) techniques.

7. REFERENCES

[1] Cornelis N de Graaf, Andr´e SE Koster, Koen L Vincken, and Max A Viergever. Validation of the interleaved pyramid for the segmentation of 3d vector images. Pattern Recognition Letters,15(5):469–475, 1994.

[2] William R Crum, Thomas Hartkens, and DLG Hill. Non-rigid image registration: theory and practice. The British Journal of Radiology, 2014.

[3] Barbara Zitova and Jan Flusser. Image registration methods: a survey. Image and vision computing, 21(11):977–1000, 2003.

[4] Terry Peters and Kevin Cleary. Image-guided interventions: technology and applications. Springer Science & Business Media, 2008.

[5] Matthew A Mauro, Kieran PJ Murphy, Kenneth R Thomson, Anthony C Venbrux, and Robert A Morgan. Image-guided interventions: expert radiology series. Elsevier Health Sciences, 2013.

[6] David Jaffray, Patrick Kupelian, Toufik Djemil, and Roger M Macklis. Review of image-guided radiation therapy. Expert review of anticancer therapy, 7(1):89–103, 2007.

[7] Marc R Mayberg, Eric LaPresto, and Edwin J Cunningham. Image-guided endoscopy: description of technique and

potential applications. Neurosurgical focus, 19(1):1–5, 2005.

[8] Primoz Markelj, Dejan Tomaˇzeviˇc, Bostjan Likar, and Franjo Pernuˇs. A review of 3d/2d registration methods for image-guided interventions. Medical image analysis, 16(3):642–661, 2012.

[9] Mark Fisher, Christopher Applegate, Mohammad Ryalat, Stephen Laycock, Mark Hulse, Daniel Emmens, Duncan Bell, et al. Evaluation of 3-d printed immobilization shells for head and neck IMRT. Open Journal of Radiology, 4(04):322, 2014.

[10] Graeme M Campbell, Sanjay Tiwari, Friederike Grundmann, Nicolai Purcz, Christian Schem, and Claus-C Gl¨uer. Three-dimensional image registration improves the long-term precision of in vivo micro-computed tomographic measurements in anabolic and catabolic mouse models. Calcified tissue international, 94(3):282–292, 2014.

[11] Dinesh D Patil and Sonal G Deore. Medical image segmentation: a review. International journal of computer science and mobile computing, 2(1):22–27, 2013.

[12] Yousef Rezaeitabar and Ilkay Ulusoy. Automatic 3d segmentation of individual facial muscles using unlabeled prior information. International journal of computer assisted radiology and surgery, 7(1):35–41, 2012.

[13] Zhen Ma, Joˇao Manuel RS Tavares, Renato Natal Jorge, and T Mascarenhas. A review of algorithms for medical image segmentation and their applications to the female pelvic cavity. Computer Methods in Biomechanics and Biomedical Engineering, 13(2):235–246, 2010.

[14] William R Crum, Oscar Camara, and Derek LG Hill. Generalized overlap measures for evaluation and validation in medical image analysis. IEEE transactions on medical imaging, 25(11):1451–1461, 2006.

[15] Emran Mohammad Abu Anas, Abtin Rasoulian, Alexander Seitel, Kathryn Darras, David Wilson, Paul St John, David Pichora, Parvin Mousavi, Robert Rohling, and Purang Abolmaesumi. Automatic segmentation of wrist bones in ct using a statistical wrist shape + pose model. IEEE transactions on medical imaging, 35(8):1789–1801, 2016.

[16] Niansong Ye, Hu Long, Junjie Xue, Sheng Wang, Xin Yang, and Wenli Lai. Integration accuracy of laser-scanned dental models into maxillofacial cone beam computed tomography images of different voxel sizes with different segmentation threshold settings. Oral surgery, oral medicine, oral pathology and oral radiology, 117(6):780–786, 2014.

[17] Massimo Martorelli, Pietro Ausiello, and Renato Morrone. A new method to assess the accuracy of a cone beam computed tomography scanner by using a non-contact reverse engineering technique. Journal of dentistry, 42(4):460–465, 2014.

[18] Xin Liang et al. A comparative evaluation of cone beam computed tomography (CBCT) and multi-slice CT (MSCT). part II: On 3D model accuracy. European journal of radiology, 75(2):270–274, 2010.

[19] Bong Chul Kim, Chae Eun Lee, Wonse Park, Sang Hoon Kang, Piao Zhengguo, Choong Kook Yi, and Sang-Hwy Lee. Integration accuracy of digital dental models and 3-dimensional computerized tomography images by sequential point-and surface-based markerless registration. Oral Surgery, Oral Medicine, Oral Pathology, Oral Radiology, and Endodontology, 110(3):370–378, 2010.

[20] Hoon Noh, Wael Nabha, Jin-Hyoung Cho, and Hyeon-Shik Hwang. Registration accuracy in the integration of laser-scanned dental images into maxillofacial cone-beam computed tomography images. American Journal of Orthodontics and Dentofacial Orthopedics, 140(4):585–591, 2011.

[21] Niansong Ye, Hu Long, Songsong Zhu, Yunqiang Yang, Wenli Lai, and Jing Hu. The accuracy of computer image-guided template for mandibular angle ostectomy. Aesthetic plastic surgery, 39(1):117–123, 2015.

[22] Pietro Ausiello, Stefano Ciaramella, Franklin Garcia-Godoy, Antonio Gloria, Antonio Lanzotti, Saverio Maietta, and Massimo Martorelli. The effects of cavitymargin- angles and bolus stiffness on the mechanical behavior of indirect resin composite class ii restorations. Dental Materials, 33(1):e39–e47, 2017.

[23] Daniel P. Huttenlocher, Gregory A. Klanderman, and William J Rucklidge. Comparing images using the hausdorff distance. IEEE Transactions on pattern analysis and machine intelligence, 15(9):850–863, 1993.

[24] Manuel Pinheiro and JL Alves. A new level-set-based protocol for accurate bone segmentation from CT imaging. IEEE Access, 3:1894–1906, 2015.

[25] Bernhard Preim and Dirk Bartz. Visualization in medicine: theory, algorithms, and applications. Morgan Kaufmann, 2007.

[26] Krit Somkantha, Nipon Theera-Umpon, and Sansanee Auephanwiriyakul. Boundary detection in medical images using edge following algorithm based on intensity gradient and texture gradient features. IEEE transactions on biomedical engineering, 58(3):567–573, 2011.

[27] Peter C Tay, Christopher D Garson, Scott T Acton, and John A Hossack. Ultrasound despeckling for contrast enhancement. IEEE Transactions on Image Processing,19(7):1847–1860, 2010.

[28] Jan Egger, Tina Kapur, Andriy Fedorov, Steve Pieper, James V Miller, Harini Veeraraghavan, Bernd Freisleben, Alexandra Golby, Christopher Nimsky, and Ron Kikinis. Gbm volumetry using the 3d slicer medical image computing platform. arXiv preprint arXiv:1303.0964, 2013.

[29] Abdel Aziz Taha and Allan Hanbury. Metrics for evaluating 3d medical image segmentation: analysis, selection, and tool. BMC medical imaging, 15(1):29, 2015.

[30] Pankaj K Agarwal, Sariel Har-Peled, Micha Sharir, and Yusu Wang. Hausdorff distance under translation for points and balls. ACM Transactions on Algorithms (TALG), 6(4):71, 2010.

[31] Sun-Jeong Kim, Soo-Kyun Kim, and Chang-Hun Kim. Discrete differential error metric for surface simplification. In Computer Graphics and Applications, 2002. Proceedings. 10th Pacific Conference on, pages 276–283. IEEE, 2002.

[32] ABLE SOFTWARE CORP. http://www.ablesw.com/3d-doctor/format.html. Accessed: 19-01-2017.

[33] The Biomedical 3D Printing Community (embodi3D LLC). https://www. embodi3d.com/. Accessed: 19-01-2017.

[34] Kenneth Clark et al. The cancer imaging archive (TCIA): maintaining and operating a public information repository. Journal of digital imaging, 26(6):1045–1057, 2013.

[35] The Cancer Imaging Archive. http://doi.org/10.7937/K9/TCIA.2015. 7AKGJUPZ/. Bosch, Walter R. and Straube, William L. and Matthews, John W. and Purdy, James A. Data From Head Neck Cetuximab (2015).

[36] Steven M Seitz, Brian Curless, James Diebel, Daniel Scharstein, and Richard Szeliski. A comparison and evaluation of multi-view stereo reconstruction algorithms. In Computer vision and pattern recognition, 2006 IEEE Computer Society Conference on, volume 1, pages 519–528. IEEE, 2006.

[37] Joseph B Anstey, Erin Janine Smith, Brian Rasquinha, John F Rudan, and Randy E Ellis. On the use of laser scans to validate reverse engineering of bony anatomy. In MMVR, pages 18–24, 2011.

[38] Thabo Beeler, Bernd Bickel, Paul Beardsley, Bob Sumner, and Markus Gross. High-quality single-shot capture of facial geometry. In ACM Transactions on Graphics (ToG), volume 29, page 40. ACM, 2010.

[39] Eero Huotilainen, Risto Jaanimets, Ji˘r´ı Val´a˘sek, Petr Marci´an, Mika Salmi, Jukka Tuomi, Antti M¨akitie, and Jan Wolff. Inaccuracies in additive manufactured medical skull models caused by the dicom to stl conversion process. Journal of Cranio- Maxillofacial Surgery, 42(5):e259–e265, 2014.

[40] Ryalat, Mohammad Hashem, Hussam N. Fakhouri, Jamal Zraqou, Faten Hamad, and Mamon S. Alzboun. "Enhanced Multi-Verse Optimizer (TMVO) and Applying it in Test Data Generation for Path Testing." International Journal of Advanced Computer Science and Applications 14, no. 2 (2023).

[41] SD Laycock, M Hulse, CD Scrase, MD Tam, S Isherwood, DB Mortimore, D Emmens, J Patman, SC Short, and GD Bell. Towards the production of radiotherapy treatment shells on 3d printers using data derived from dicom ct and mri: preclinical feasibility studies. Journal of Radiotherapy in Practice, 14(01):92–98, 2015.

[42] Mohammad Hashem Ryalat, Daniel Emmens, Mark Hulse, Duncan Bell, Zainab Al-Rahamneh, Stephen Laycock, and Mark Fisher. Evaluation of particle swarm optimisation for medical image segmentation. In International Conference on Systems Science, pages 61–72. Springer, 2016.

[43] Zacharias Fourie, Janalt Damstra, Peter O Gerrits, and Yijin Ren. Evaluation of anthropometric accuracy and reliability using different three-dimensional scanning systems. Forensic Science International, 207(1):127–134, 2011.

[44] Niansong Ye, Fan Jian, Junjie Xue, Sheng Wang, Lina Liao, Wenya Huang, Xing Yang, Yang Zhou, Wenli Lai, Jingtao Li, et al. Accuracy of in-vitro tooth volumetric measurements from cone-beam computed tomography. American Journal of Orthodontics and Dentofacial Orthopedics, 142(6):879–887, 2012.

[45] M Dahmani-Causse, M Marx, O Deguine, B Fraysse, B Lepage, and B Escud´e. Morphologic examination of the temporal bone by cone beam computed tomography: comparison with multislice helical computed tomography. European annals of otorhinolaryngology, head and neck diseases, 128(5):230–235, 2011.

[46] Ryalat, Mohammad Hashem, Stephen Laycock, and Mark Fisher. "A fast and automatic approach for removing artefacts due to immobilisation masks in X-ray CT." In 2017 IEEE EMBS International Conference on Biomedical & Health Informatics (BHI), pp. 33-36. IEEE, 2017.

[47] Ryalat, Mohammad Hashem, Stephen Laycock, and Mark Fisher. "Automatic removal of mechanical fixations from CT imagery with particle swarm optimisation." In Bioinformatics and Biomedical Engineering: 5th International Work-Conference, IWBBIO 2017, Granada, Spain, April 26–28, 2017, Proceedings, Part I 5, pp. 419-431. Springer International Publishing, 2017.